Applied Energy 369 (2024) 123528

Contents lists available at ScienceDirect

Applied Energy

journal homepage: www.elsevier.com/locate/apenergy

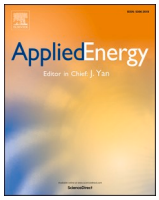

Dual electromagnetic mechanisms with internal resonance for ultra-low frequency vibration energy harvesting

Ruqi Sun [a], Shengxi Zhou [b,*], Zhongjie Li [c,*], Li Cheng [d]

[a] School of Automobile, Chang'an University, Xi'an 710018, China
[b] School of Aeronautics, Northwestern Polytechnical University, Xi'an 710072, China
[c] School of Mechatronic Engineering and Automation, Shanghai University, Shanghai 200444, China
[d] Department of Mechanical Engineering, The Hong Kong Polytechnic University, Hong Kong 990777, China

HIGHLIGHTS

- Dual electromagnetic meachanisms enable watt-level output power.
- Pendulum swinging amplitude is restricted with even larger ouput power.
- Internal resonance for frequency up-conversion is realized.

ARTICLE INFO

Keywords:
Electromagnetic energy harvester
Internal resonance
Electromagnetic shunt damping
Spring pendulum

ABSTRACT

Ultra-low frequency vibration in ambient environment is an abundant renewable energy source. Corresponding energy harvesters have attracted increasing attention from both academic and industrial worlds. In this paper, a rotational electromagnetic energy harvester (EMEH) and a translational EMEH are combined into a spring pendulum system, thus forming a dual EMEH, in which internal resonance phenomenon is triggered to result in significantly enhanced energy harvesting efficiency. The spring pendulum system exhibits robustness and stability with the equivalent electromagnetic shunt damping constraints. Meanwhile, the tunable damping preserves the integrity of the system even the external excitation overloads. Experimental results demonstrate that the output power of the dual EMEHs can reach up to 0.9 W with a moving mass of 1.42 kg. Moreover, the swing angle of the pendulum can be reduced with the effect of internal resonance, which protects the main system and ensures its operation in harsh operating environment.

1. Introduction

Ocean wave oscillation is a typical ultra-low frequency vibration source, which contains abundant energy that can be harvested. Scruggs and Jacob [1] analyzed the considerable amount of power contained in ocean waves and stated the engineering challenges for harvesting energy. Aderinto and Li [2] assessed the ocean wave energy resource, reviewed commonly used wave energy extraction technologies, and discussed challenges for industrial application. On the same topic, Sun et al. [3] reviewed the existing enhancement techniques of various energy harvesters. As for the harvesting principles, the piezoelectric energy harvester (PEH) [4], the electromagnetic energy harvester (EMEH) [5], the triboelectric nanogenerators (TENG) [6], and various combinations of the three kinds of harvesters [7] with proper interface circuit [8] were extensively exploited and widely used by both researchers and industrial practitioners. Different structural design and optimization methods are proposed to reach high efficiency of ultra-low frequency vibration energy harvesting, including the quasi-zero-stiffness (QZS) technique, multistable energy harvesters, pendulum structures, etc.

QZS technique is one of the most researched topics recently for various applications including vibration isolation [9–12]. QZS-based energy harvesting [13,14] recently emerged as a hot topic, such as bio-inspired QZS energy harvesters [15,16], bi-objective QZS designs with simultaneous vibration control and energy harvesting function [17], etc. The latter was reviewed by Chen et al. [18], commenting on different bi-objective QZS designs realized in recent years. Multistable vibration energy harvester is another hot research topic for ultra-low frequency energy harvesting. Corresponding research ranges from monostable systems to bistable, tristable, and multistable systems. The

* Corresponding authors.
E-mail addresses: zhoushengxi@nwpu.edu.cn (S. Zhou), lizhongjie@shu.edu.cn (Z. Li).

https://doi.org/10.1016/j.apenergy.2024.123528
Received 12 December 2023; Received in revised form 2 April 2024; Accepted 20 May 2024
Available online 30 May 2024

Nomenclature

DAS	Data acquisition station
DOF	Degree-of-freedom
EMEH	Electromagnetic energy harvester
FFT	Fast Fourier transform
PEH	Piezoelectric energy harvester
QZS	Quasi-zero-stiffness
TENG	Triboelectric nanogenerators

main purpose is to ensure effective operation of the harvesters subjected to ultra-low frequency excitations. In this regard, Fan et al. [19] designed a monostable system with special magnet arrangement, which can effectively lower the PEH response to a lower frequency range. Erturk and Inman [20] proposed a bistable Duffing oscillator to obtain high-energy orbits without resonance consideration. Zhou et al. [21–23] designed several bio-inspired bow-type bistable PEHs, with corresponding effective low working frequency verified by experiments. Liu et al. [24] developed a bistable nonlinear stiffness identification method to predict and enhance the system working performance. A broadband tristable energy harvester was also modeled and experimentally verified [25]. While most above harvesters were designed in symmetric structural form, the asymmetric type bistable [26] and tristable energy harvesters [27] were also analyzed, and corresponding high-energy orbits were compared with the symmetric structures. For multistable energy harvesters, Zhou et.al [28,29] reviewed the state-of-art progress in modeling principles, performance enhancement, and design methods. Alternative designs without external magnets [30], calculating methods of magnetic force [31], multistable energy harvesters with rolling magnets [32], and pendulum [33] were also considered in view of enhancing the performance of multistable energy harvesters. Recently, more diversified energy harvesting structures were proposed to harvest the ultra-low frequency vibration energy. For example, Song et al. [34] proposed two tandem cylinder PEHs to harvest water flow energy. With a gravity-driven roller, Zhao et al. [35] used a bio-inspired structure to cope with the ultra-low frequency vibration energy, and used the harvested energy to power ocean environment monitoring sensors. Shen et al. [36] used inerter-based EMEH to mitigate the vibration of a bridge stay cable, and achieve simultaneous vibration energy harvesting in the system. Tan et al. [37] proposed a string-suspended rotor to implement the frequency up-conversion mechanism that leads to a significant enhancement of energy harvesting efficiency. Ma et al. [38] leverage the magnets-enabled snap-through phenomenon to achieve the vibration-rotation modulation.

Moreover, the ultra-low natural frequency feature of the pendulum-like structure is potentially conducive to ultra-low frequency vibration energy harvesting. Typical designs include planar pendulum [39], spherical pendulum [40], double pendulum [41], etc. Wang [42] reviewed the research progress on pendulum-based energy harvesters. Design types, modulation mechanisms, transducer selections, characteristics, performance, and applications were objectively compared among different pendulum harvesters. Meanwhile, internal resonance principle has been widely investigated to reach a wider working band and higher frequency range for energy harvesting. Related works include Chen and Jiang [43] which utilized the internal resonance phenomenon to fabricate an EMEH with snap-through nonlinearity. Clamped-clamped beams with a mounted oscillator [44] were regarded as a typical case for internal resonance harvesting. Cantilever pendulum structure [45] was also proved effective in collecting multi-direction excited vibration energy. Double beams were utilized to achieve internal resonance in which the energy of the main beam can be transferred into the auxiliary beam [46,47].

Combining the pendulum and internal resonance phenomenon, the spring pendulum proves to be an effective design for ultra-low frequency vibration energy harvesting. Compared with aforementioned beam-based internal resonance harvesters, a simple spring pendulum, as a nonlinear structure, can be applied in real engineering sites more easily. Corresponding modeling and response characteristics have been proposed and investigated for a long time. For example, Kane and Kahn [48] obtained the resonance boundary conditions and studied characteristics of resonant oscillations. Narkis [49] and Miles [50] analyzed the spring pendulum stability and verified the 1:2 internal resonance phenomenon. Broucke and Baxa [51] gave the periodic solutions of a spring pendulum with periodic orbits methods. Gitterman [52] investigated the spring pendulum system response with parametric excitation and external force. Recently, some new modeling and analysis methods for spring pendulum motion solutions are still emerging. Baleanu et al. [53] used the fractional model to describe the spring pendulum motion, which can excavate more hidden information of the physical world. Abohamer et al. [54] analyzed the steady-state asymptotic motion response and stability with both piezoelectric and electromagnetic devices. Souda et al. [55] explored the energy distribution of the spring pendulum system to propose the global characteristics of the spring pendulum energy exchange by considering a great number of trajectories. Amer et al. [56,57] used the multiple scales method to explore the chaotic response of a circular spring pendulum with harmonic excitation. Even for a simple nonlinear system, the uncertain dynamics deserve further exploration.

Referring to energy harvesting with the spring pendulum, more and more research has been conducted currently due to its ultra-low frequency applicability. Kecik and Borowiec [58] explored the auto-parametric response of a pendulum with vertical excitation, and proposed simulation results for various pendulum motion types. Mitura and Kecik [59,60] analyzed the parameters that influence the energy harvesting efficiency and conducted experiments to verify the theoretical results. Jiang et al. [61] evaluated the improvement of bandwidth with the analysis of the nonlinear behavior. To harvest the ultra-low frequency vibration energy, Wu et al. [62] designed a multi-direction spring pendulum like PEH by capitalizing on 1:2 internal resonance, then a 1:2:6 frequency up-conversion mechanism [63] was used to obtain higher energy harvesting efficiency. The spring pendulum system with internal resonance phenomenon can also be regarded as a rotational mutation of the translational dynamic vibration absorber (DVA). He et al. [64] used multiple scales method to obtain the bi-objective of vibration control and energy harvesting with precise results. Kecik and Mitura [65–67] then studied the pendulum absorber with simultaneous energy harvesting function, corresponding experiments were conducted to verify the energy harvesting performance without decreasing the vibration reduction effectiveness.

With the aforementioned spring pendulum based energy harvesters, the increase in the effective bandwidth is clear, and the vibration mitigation performance can also be guaranteed with properly designed structural parameters. However, the achieved harvested energy is still at the milliwatt level (mW), which can only be used to power some low-power sensors. When used for more power-demanding electrical appliances, the harvested energy is usually not enough, particularly for the offshore operating environment with limited power supply. To tackle this problem, this paper proposes dual EMEHs with internal resonance to harvest ultra-low frequency (lower than 1 Hz) vibration energy. The contribution of this work is mainly twofold: (1) realization of high output power up to Watt level with high energy density; (2) containment of the pendulum swing amplitude to a relatively low level.

The proposed system is designed for ocean wave energy harvesting, particularly for the buoy internal installation. The ocean wave excitation features ultra-low frequency and large amplitude for which the proposed pendulum structure can then take the best advantage. Moreover, the spring pendulum system is shown to be effective in improving the output frequency without complex structural design. In the following sections, the design and the modeling of the proposed mechanism are illustrated

in Section 2. Experimental setup and parameter identifications are given in Section 3. Then the results are discussed in Section 4. Section 5 summarizes the main conclusions.

2. Design and modeling

In this section, the proposed dual EMEHs in a spring pendulum structure with internal resonance alongside an EMEH in a single pendulum structure used as a comparison are illustrated. Corresponding models with rotational damping are established to predict the two kinds of motion trajectories and output voltage.

2.1. EMEH with internal resonance

A rotational EMEH and a translational EMEH are combined in a spring pendulum structure as shown in Fig. 1(a). The rotational EMEH, later labeled as H_1, is composed of a gearbox for frequency up-conversion, a permanent magnet DC motor that is used for electricity generation, and a tunable potentiometer for changing the load resistance. The rotating shaft of the gearbox is connected to the pendulum axis so that the swing energy can be harvested into the rotational EMEH.

The translational EMEH, later labeled as H_2, is a specifically designed electromagnetic transducer with opposing magnet pairs to achieve maximum transduction factor. The number of opposing magnet pairs is optimized as four to reach the highest electromechanical coupling performance with the structural parameter's limitation [68]. The coil is fixed at the pendulum axis, while the opposing magnet bar is connected with the pendulum axis through a spring, while the other end is hanging a counter-weight mass. Therefore, the dual EMEHs contain two energy sources, H_1 and H_2, which can be simplified as a two degree-of-freedom (DOF) system as shown in Fig. 2(a). With a horizontal excitation, the swing pendulum drives H_1 to rotate and H_2 to vibrate in the radial direction. As a result, both EMEHs can harvest the ultra-low frequency vibration energy, whose efficiency can be maximized through a proper tuning of the natural frequencies of the system by adjusting the swing pendulum and spring-mass parameters.

Moreover, the comparative single pendulum harvester in Fig. 1(b) is a one DOF system with the magnets and coils of H_2 fixed together. With an external excitation, the system will only swing so that H_1 can work and harvest energy, but H_2 can be regarded as a proof mass of swinging H_1. Without the participation of H_2, the measured response results allow the identification of H_1 parameters.

2.2. Theoretical analysis

Both aforementioned designs can be modeled by the simplified motion models shown in Fig. 2. Since the coil weight of H_2 is non-negligible when compared with the weight of the spring-mass oscillator, the weight of H_2 coil and the boned tube is regarded as a concentrated mass m_1. m_2 is the equivalent weight of the spring-mass oscillator. The coordinate origin is selected at the rotating shaft in the swing plane. c_1 and c_2 are the equivalent damping coefficients of rotational H_1, and the translational H_2, respectively. k is the spring stiffness of translational vibration system, l_1 is the distance between the origin and m_1 center of gravity, which is a constant for both static and dynamic cases. l_2 denotes the distance between the origin and m_2 with unstretched spring. The distance between the origin and m_2 is changing due to the spring deformation, denoted by r. The swing angle is denoted by θ, and the whole system is excited by a displacement s in the horizontal direction.

The degenerative one DOF system can be modeled with a simple swing pendulum as shown in Fig. 2(b). The concentrated mass m is calculated by adding up m_1 and m_2. The distance l can be measured between the origin and the mass center of gravity. The remaining symbols are the same as the spring pendulum system. To obtain the system response under different inputs of both kinds of designs, the second kind of Lagrange's equation is used:

$$\frac{d}{dt}\left(\frac{\partial T}{\partial \dot{q}}\right)-\frac{\partial T}{\partial q}+\frac{\partial U}{\partial q}+\frac{\partial D}{\partial \dot{q}}=0 \tag{1}$$

where T is the kinetic energy, U is the potential energy, D is the dissipative power, q is the independent coordinates necessary to describe the system's motion at any instant. The detailed expression of each symbol in both systems will be deduced in the next subsections.

2.2.1. Damped spring pendulum

For the damped spring pendulum system in Fig. 2(a), the kinetic energy, potential energy, and dissipative power can be written as:

$$T=\frac{1}{2}m_1\left[\left(\dot{x}_1-\dot{s}\right)^2+\dot{y}_1^2\right]+\frac{1}{2}m_2\left[\left(\dot{x}_2-\dot{s}\right)^2+\dot{y}_2^2\right] \tag{2}$$

$$U=m_1gy_1+m_2gy_2+\frac{1}{2}k\left(r+\frac{m_2g}{k_2}\right)^2 \tag{3}$$

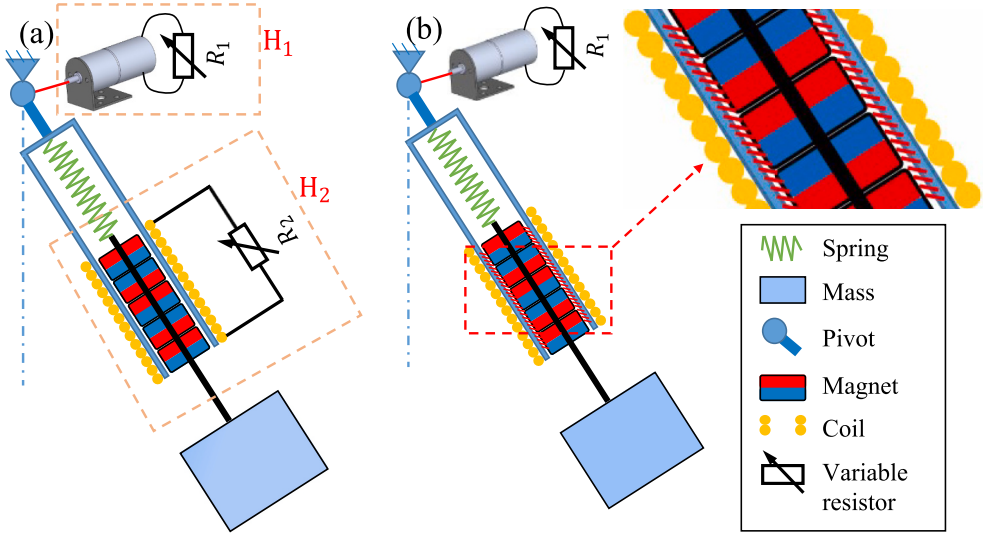

Fig. 1. Structure design with a rotational EMEH (H_1) and translational EMEH (H_2): (a) Dual EMEHs in spring pendulum structure; (b) one harvester (H_1) with single pendulum response only.

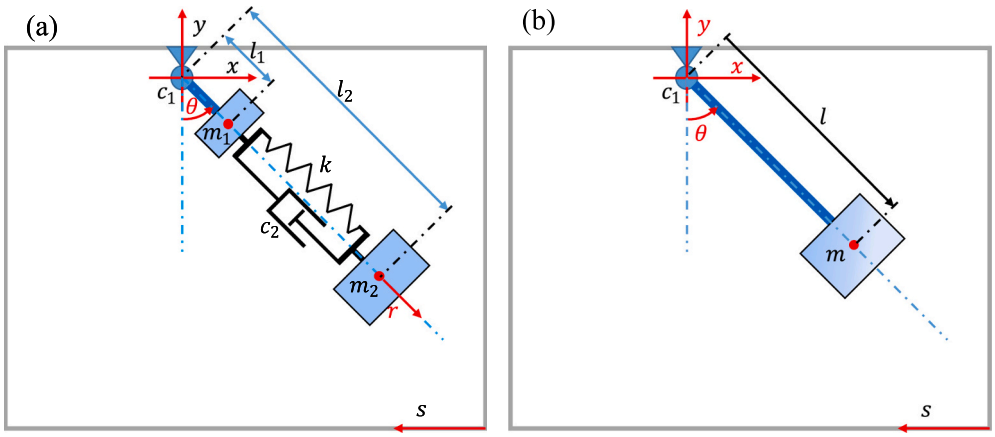

Fig. 2. Simplified motion model: (a) Spring pendulum; (b) single pendulum.

$$D = \frac{1}{2}c_1\dot{\theta}^2 + \frac{1}{2}c_2\dot{r}^2 \tag{4}$$

where the positions of m_1 and m_2 in Cartesian coordinate can be described as follows:

$x_1 = l_1 sin\theta,\ \dot{x}_1 = l_1 cos\theta \bullet \dot{\theta}.$

$y_1 = -l_1 cos\theta,\ \dot{y}_1 = l_1 sin\theta \bullet \dot{\theta}$

$x_2 = (l_2 + r)sin\theta,\ \dot{x}_2 = (l_2 + r)cos\theta \bullet \dot{\theta} + \dot{r} \bullet sin\theta$

$y_2 = -(l_2 + r)cos\theta,\ \dot{y}_2 = (l_2 + r)sin\theta \bullet \dot{\theta} - \dot{r} \bullet cos\theta$

For the coordinate θ, taking all the variables and realtions into Eq. (1) yields:

$$\left[m_1 l_1^2 + m_2(l_2 + r)^2\right]\ddot{\theta} - [m_1 l_1 + m_2(l_2 + r)]cos\theta\ddot{s} + 2m_2(l_2 + r)\dot{r}\dot{\theta} + m_1 g l_1 sin\theta + m_2 g(l_2 + r)sin\theta + c_1\dot{\theta} = 0 \tag{5}$$

For the coordinate r, taking all the variables and realtions into Eq. (1) yields:

$$m_2\ddot{r} - m_2\ddot{s}sin\theta - m_2(l_2 + r)\dot{\theta}^2 + kr + m_2 g - m_2 g cos\theta + c_2\dot{r} = 0 \tag{6}$$

The detailed relations derivation of variables are shown in Appendix A. The final explicit expressions of Eqs. (5) and (6) are:

$$\ddot{\theta} = \frac{1}{m_1 l_1^2 + m_2(l_2 + r)^2}\left\{[m_1 l_1 + m_2(l_2 + r)]cos\theta\ddot{s} - 2m_2(l_2 + r)\dot{r}\dot{\theta} - m_1 g l_1 sin\theta - m_2 g(l_2 + r)sin\theta - c_1\dot{\theta}\right\} \tag{7}$$

$$\ddot{r} = \ddot{s}\,sin\theta + (l_2 + r)\dot{\theta}^2 - \frac{k}{m_2}r + g(cos\theta - 1) - \frac{c_2}{m_2}\dot{r} \tag{8}$$

2.2.2. Damped single pendulum

For the degenerated single pendulum system in Fig. 2(b), only one DOF exists with the moving mass $m = m_1 + m_2$. Corresponding kinetic energy, potential energy, and the dissipative power can be written as:

$$T = \frac{1}{2}m\left[(\dot{x} - \dot{s})^2 + \dot{y}^2\right] \tag{9}$$

$$U = -mglcos\theta \tag{10}$$

$$D = \frac{1}{2}c_1\dot{\theta}^2 \tag{11}$$

where the positions of m in Cartesian coordinate can be written as:

$x = lsin\theta,\ \dot{x} = lcos\theta \bullet \dot{\theta}$

$y = -lcos\theta,\ \dot{y} = lsin\theta \bullet \dot{\theta}$

With the detailed relations derivation in Appendix B, Eq. (1) can be transferred as:

$$ml^2\ddot{\theta} - mlcos\theta \bullet \ddot{s} + mglsin\theta + c_1\dot{\theta} = 0 \tag{12}$$

The explicated expressions of Eq. (12) can be written as:

$$\ddot{\theta} = \frac{1}{l}cos\theta \bullet \ddot{s} - \frac{g}{l}sin\theta - \frac{c_1}{ml^2}\dot{\theta} \tag{13}$$

3. Experimental setup and parameter identifications

To verify the energy harvesting performance and theoretical analyses, a prototype of dual EMEHs is fabricated and settled on an ultra-low frequency vibration exciter for the test. Corresponding model parameter identification process is also elaborated in this section.

3.1. Experimental setup

The experimental system is built as shown in Fig. 3 to implement the design model in Fig. 1. A linear motor with the capacity of providing ultra-low frequency motion is used as the exciter. Relative motor driver and control box are used to control the excitation types.

A prototype with dual EMEHs in a spring pendulum structure is fabricated and fixed on a holder, which is connected with the mover of the linear motor. External resistors R_1 and R_2 are used to tune the matching resistance and count the output power of H_1 and H_2. As shown in Fig. 3(b), the stator of rotational H_1 is fixed on the stator, while the rotor is connected with the pendulum rotating shaft. An angular displacement sensor is also boned with the pendulum rotating shaft to measure the pendulum swing angle. The coil of the translational H_2 bonded with the pendulum, and the magnets bar plays as part of moving mass m_2 of the spring-mass oscillator system in Fig. 3(c). A laser displacement sensor is fixed on the coil that also contributes to m_1. After tuning the relative position between the magnets bar and the coil to ensure proper coupling when the spring is stretched with gravity, two limit circular plates in Fig. 3(d) are used to restrict the vibration amplitude so that H_2 operates in an effective range. The two displacement sensors, and the external resistors R_1 and R_2 are connected to a data acquisition station (DAS) so that the response and the output power can be measured. The related converter parameters of both H_1 and H_2 are listed in Table 1.

3.2. Model parameter identification

The hand-measured structural parameters usually contain accumulated errors for the performance evaluation. The parameter identification based on the sensor-measured signals can highly improve the reliability of the proposed model. For the dual EMEHs, the natural frequency, matching resistance, and corresponding damping coefficients of H_1 and H_2 are dominant parameters to be identified.

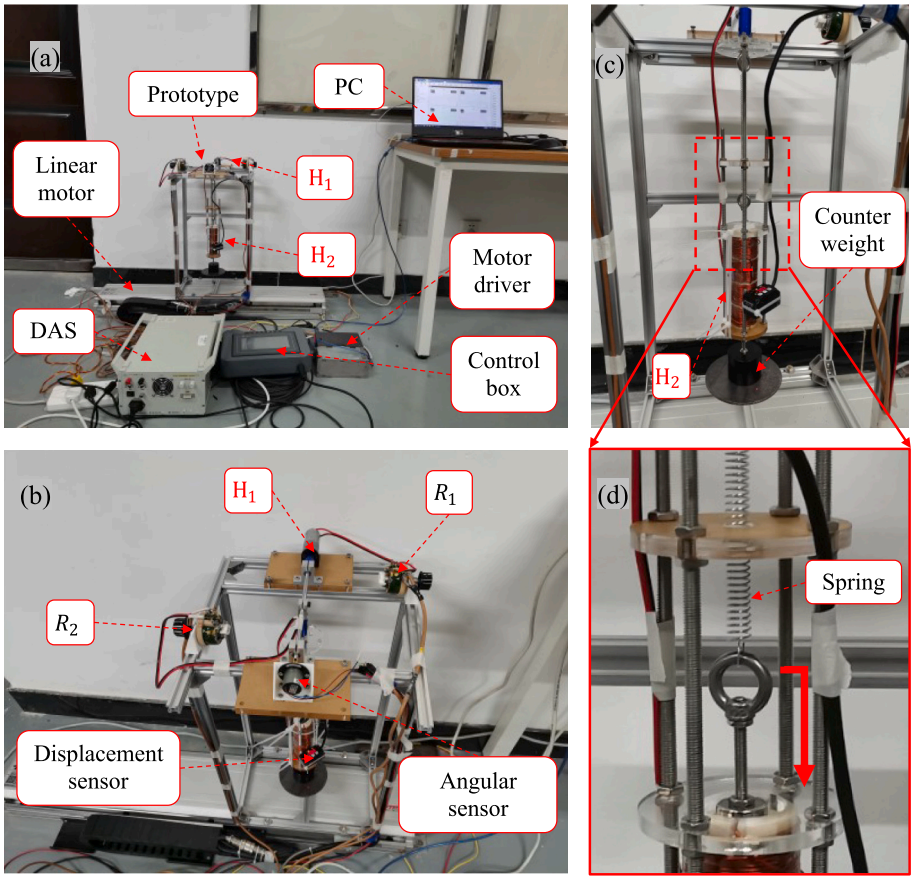

Fig. 3. Experimental setup: (a) Overview; (b) rotational EMEH H_1; (c) linear EMEH H_2; (d) detailed spring of H_2.

Table 1
Converter parameters of H_1 and H_2.

Converter	Parameter	Value
H_1	Length	53.8 mm
	Diameter	24.4 mm
	Gear ratio	78
	Stator resistance	37.5 Ω
	Speed constant	4.9 mV/rpm
H_2	Length	120 mm
	Diameter	32 mm
	Coil resistance	1.5 Ω
	Transduction factor	6.522 V•s/m

3.2.1. *Natural frequency*

The natural frequency of the swinging pendulum and the spring mass oscillator can be easily obtained through the free vibration response curves with both harvester coils set in open circuit conditions. When the second DOF is blocked by adding cable ties to bond the magnet bar and the coil as shown in Fig. 3(c), the pendulum swinging free response curve can be obtained as shown in Fig. 4(a). Similarly, when the rotational shaft is fixed to restrict swinging, an initial displacement excitation will trigger the free vibration response of the second DOF. The corresponding curve is plotted in Fig. 4(b). Both free vibration response curves can be described as the equation below:

$$\theta(t)\,|r(t) = e^{-\zeta\omega_n t}\left(A_1 cos\sqrt{1-\zeta^2}\,\omega_n t + A_2 sin\sqrt{1-\zeta^2}\,\omega_n t\right) \tag{14}$$

Both curves in Fig. 4 show the standard free vibration response characteristics so that the natural frequency can be identified with the

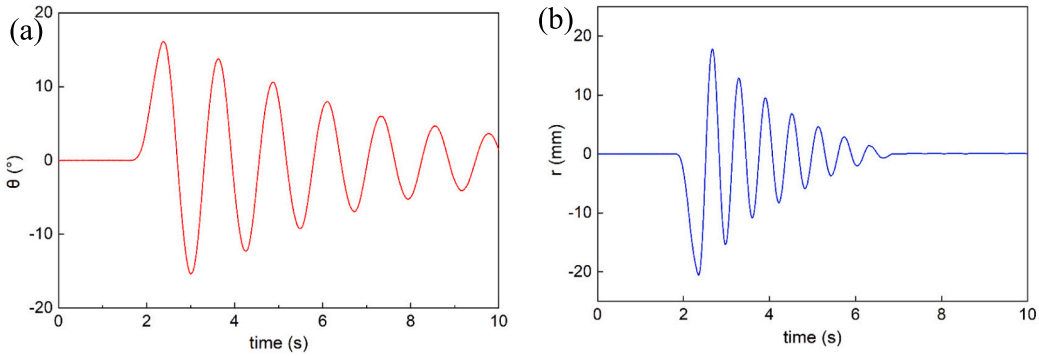

Fig. 4. Natural frequency identification of: (a) H_1 in single pendulum system; (b) H_2 in spring pendulum system with no swinging.

FFT of the obtained signals. The FFT results show that the pendulum swinging natural frequency is 0.8 Hz, and the spring mass oscillator system's natural frequency is 1.6 Hz. The natural frequency ratio is 1:2 that satisfies the internal resonance requirement as discussed in the literature.

3.2.2. Matching resistance

To achieve maximum output power, the connected external resistances of H_1 and H_2 require optimal matching. Theoretically, the optimal external resistance for maximum power [69] equals the internal resistance of EMEH coils. However, in real applications, the coil with a closed loop circuit will generate considerable heat. Therefore, the optimal matching resistance is larger than the internal resistance due to the influence of temperature and other related factors.

Prior to the starting of the optimal matching resistance test, the coil internal resistances of H_1 and H_2 are measured by a precision resistance instrument. The internal resistance of H_1 is 37.5 Ω, and that of H_2 is 1.5 Ω. Then, the output power of H_1 with variable external resistance is measured with the linear motor under the excitation frequency $f = 1$ Hz and peak-to-peak amplitude $A = 0.1$ m. The variable output power curve of H_1 with different external resistance is plotted in Fig. 5(a), which shows the maximum output power appears when external $R_1 \approx 45$ Ω. Moreover, the output power of H_2 with variable external resistance is measured with the linear motor under the excitation frequency $f = 2.5$ Hz and amplitude $A = 0.1$ m. The variable output power curve of H_2 with different external resistance is plotted in Fig. 5(b), which shows the maximum output power appears when external $R_2 \approx 2.5$ Ω. The matching resistance of both EMEHs is slightly larger than their internal resistance, which is consistent with the above analysis.

3.2.3. Rotational damping coefficient

With the assumption that the internal friction of the gearbox is negligeable, the rotational damping coefficient can be regarded to vary linearly with the circuit impedance. The rotational damping coefficient c_1 is calculated using the above selected optimal matching resistance in the single pendulum configuration to avoid the influence of internal energy alternation. The second DOF is blocked with the same methods as the pendulum natural frequency test. The external resistance R_1 is set at the matching resistance value of 45 Ω. The excitation frequency of the linear exciter is set at $f = 1$ Hz, and the excitation amplitude is varied discretely from $A = 0.025$ m to $A = 0.2$ m. Then, the swing response of the single pendulum is measured by the angular displacement sensor.

With the measured structural parameters $m = 1.4234$ kg and $l = 0.344$ m and the varied excitation amplitude, the differential equation Eq. (13) can be solved through a numerical calculation software. The swing angle in time domain with excitation amplitude $A = 0.1$ m and the swing angle amplitude with different excitation amplitudes are measured and plotted in Fig. 6 to compare with the simulation results. After tuning the damping coefficient c_1 in the calculation, the most suitable c_1 fitting the measurement is searched out at 0.3684 N•m•s/rad. As shown in Fig. 6(a), the time-domain response curve agrees well with the simulated curve in both amplitudes and phases. The measured swing angle amplitude curve with varied excitation amplitude A in Fig. 6 (b) is also consistent with the simulation results. Some internal friction and gear clearance effects may result in the deviation of several individual situations, which is also visible on the curves.

3.2.4. Translational damping coefficient

For the energy harvester H_2, the structure is a typical linear electromagnetic shunt damper for which the damping coefficient should follow linear variation. Since the matching resistance is small and the equivalent damping is rather high, free vibration response cannot last for several periods for the damping coefficient identification. The translational damping coefficient c_2 is calculated using the above selected optimal matching resistance when H_2 is under force excitation. The linear exciter in this study can only function in horizontal direction so that H_2 cannot be excited directly. Therefore, both swinging and translational DOFs are released in this test that the internal resonance occurs. The total mass m in the last rotational damping coefficient test is divided into m_1 and m_2. With the roughly measured effective length l_1 and l_2, the masses and lengths satisfy the following relationship:

$$m_1 l_1 + m_2 l_2 = (m_1 + m_2) l \tag{15}$$

In light of Eq. (15), the calculation runs with slightly ratified structural parameters. The spring stiffness k can be obtained by measuring the deformation and the changed hanging mass. The damping coefficient c_2 can be roughly estimated by referring to the calibrated transduction factor ($K_t \approx 6.522$ V•s/m) in Ref. [68].

With updated parameters, the damping coefficient c_2 is identified as 10.6 N•s/m, which is very close to the calculated value based on the transduction factor. With the identified parameters, the measured results and calculated results in terms of rotational angle θ variation with different amplitudes are in agreement as shown in Fig. 7(a) and (b). Note the measured translational displacement r variation results slightly deviate from the calculated results in Fig. 7(c) and (d). The observed difference between the measurement and calculation can be caused by factors like the air gap as well as the friction effect. Indeed, a 2 mm air gap exists between the EMEH magnets bar and the coil central hole. The laser displacement sensor is assembled parallelly to the EMEH magnets bar as shown in Fig. 3(c). However, the expected perfect parallel arrangement may not be maintained due to the air gap when the spring-mass oscillator is subjected to the centrifugal force, resulting to imprecise displacement measurement. Moreover, when the pendulum swings, the magnet might hit the internal surrounding area of the coil, thus generating contact or frictional forces which also bring error between the experiment and calculation. This might explain that fact that the measured experimental results are lower than calculated ones. Having said that, quantified analysis on the influences of the above factors is

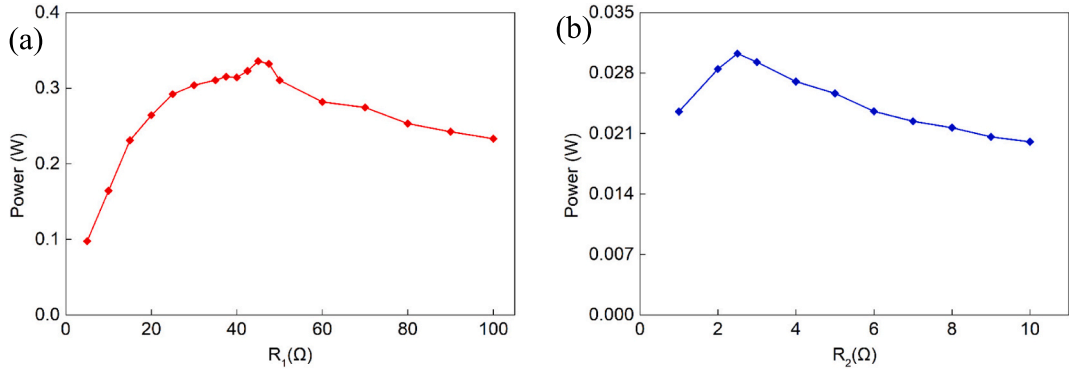

Fig. 5. Optimal external resistance matching for maximum output power of (a) H_1 and (b) H_2.

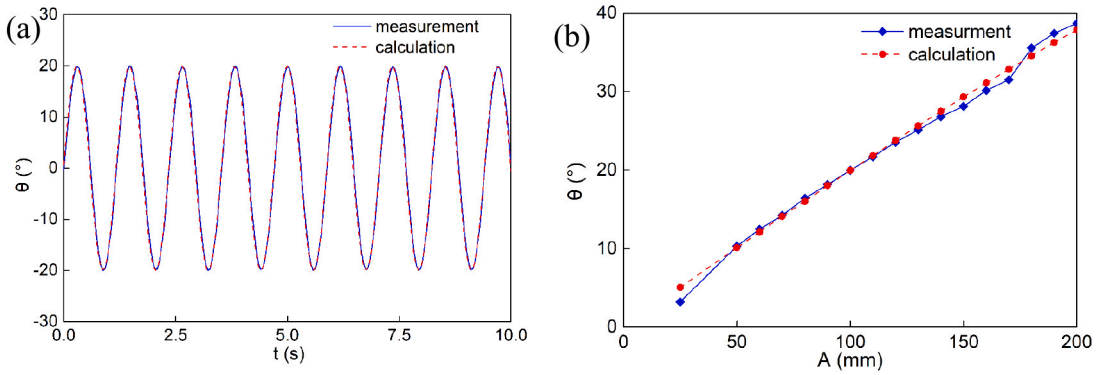

Fig. 6. Rotational damping coefficient c_1 identification in single pendulum test: (a) Rotational angle θ in time domain with the excitation amplitude $A = 0.1$ m; (b) peak value of rotational angle θ with different excitation amplitude A.

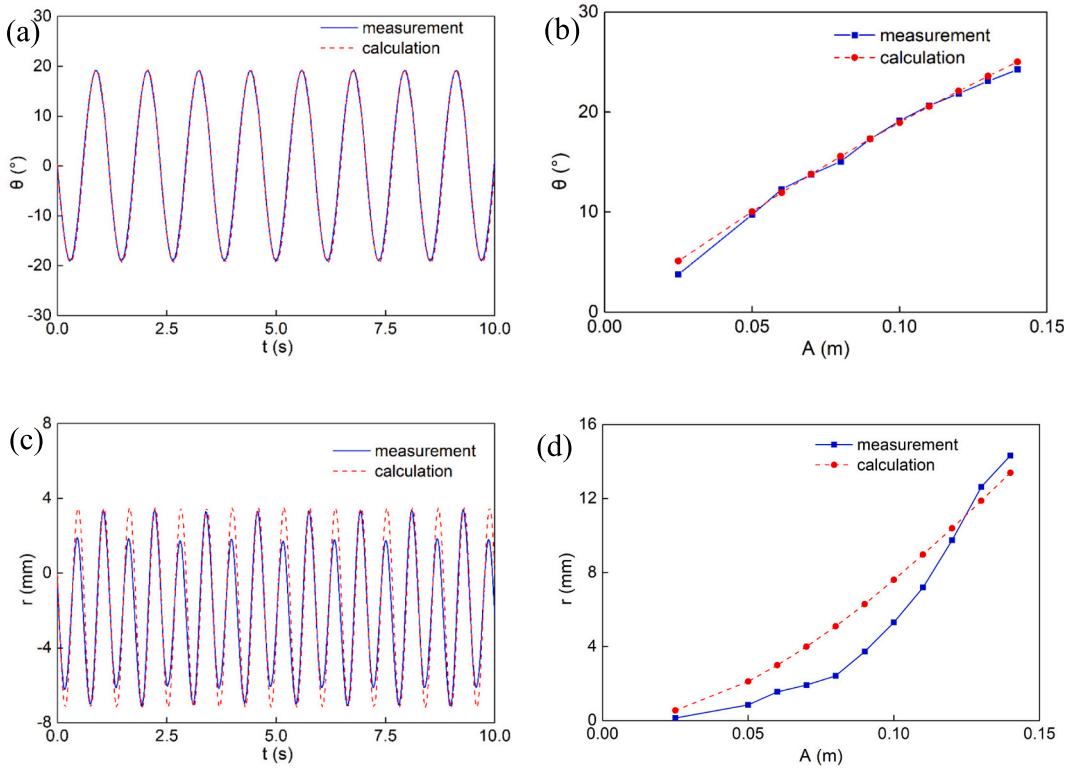

Fig. 7. Translational damping coefficient c_2 identification of: (a) Rotational angle θ in time domain with the excitation amplitude $A = 0.1$ m; (b) peak value of rotational angle θ with different excitation amplitude A; (c) translational displacement r in time domain with the excitation amplitude $A = 0.1$ m, (d) peak value of translational displacement r with different excitation amplitude A.

challenging, which deserves additional systematic work in the future.

The identified parameters of the proposed harveseters are verified with tests, and the key parameters are listed in Table 2.

Table 2
Identified parameters of both systems.

System	Notation	Value
Single pendulum	m	1.4234 kg
	l	0.344 m
Spring pendulum	m_1	0.6625 kg
	m_2	0.7609 kg
	l_1	0.31 m
	l_2	0.3736 m
	k	80.9 N/m
	c_1	0.3684 N•m•s/rad
	c_2	10.6 N•s/m

4. Experimental results and discussion

In this section, the excitation with constant acceleration and discrete sinusoidal frequency sweeping from 0.5 Hz to 5 Hz is conducted, and corresponding output power with both spring pendulum and single pendulum system is measured. Moreover, the excitation with constant sinusoidal frequency and varied amplitudes is also provided to reach the maximum output of the designed dual EMEHs.

4.1. Output with constant acceleration

Based on the relationship between the sinusoidal displacement and acceleration, the constant acceleration (0.2 g) excitation curve can be drawn and imported into the linear motor driver. The spring pendulum system and single pendulum system are both measured to assess the

performance.

4.1.1. Spring pendulum system

The output voltage of H_1 and H_2 with frequency-swept sinusoidal and constant acceleration excitation is shown in Fig. 8(a) and (b). The maximum output voltage appears around the pendulum swinging natural frequency (0.8 Hz ~ 0.9 Hz), further precisely identified as 0.85 Hz, which can be embodied in Fig. 8(c). The output voltage variation follows an increasing trend before 0.85 Hz before decreasing. An abnormal phenomenon occurs at 1.6 Hz, where the output voltage of H_1 is smaller than the ones in its adjacent frequency bands, while the output voltage of H_2 is larger. This is due to the energy transfer from the pendulum swinging to the spring mass oscillator as a result of the internal resonance phenomenon. The internal resonance phenomenon can be better seen through the output voltage comparison at 1.6 Hz in Fig. 8(a) and (b).

Under constant acceleration excitation, the output power curves of H_1 and H_2 are plotted in Fig. 8(c) and 8(d). The maximum output power of H_1 with 0.85 Hz excitation is around 398 mW, and the synchronous output power of H_2 is around 350 mW. The total output power is 0.75 W, which is sufficient for powering some sensors and low-power-demanding electrical appliances. The frequency band of H_1 is wider than that of H_2 due to their frequency response characteristics. However, H_2 can provide a double frequency output so that the frequency up-conversion can also be implemented. Moreover, the measured results match well with the calculated ones except for the lower peak value and narrower bandwidth. One plausible reason might again be the effect of the internal friction which causes lower response in the measured output power at peak and other frequencies as compared with the calculated results.

4.1.2. Single pendulum system

To compare the output performance with the above spring pendulum system, the output voltage and power of the degenerative one DOF swinging pendulum are also measured with identical excitation. As shown in Fig. 9(a), the maximum output power also locates at 0.85 Hz with a larger amplitude than that of spring pendulum system. It is worth noting that no internal resonance phenomenon exists with 1.6 Hz excitation. The maximum output power is around 0.45 W as shown in Fig. 9 (b), which is larger than that of H_1 output in the spring pendulum system, but much smaller than that of the total output of H_1 and H_2 output in spring pendulum system. Therefore, the spring pendulum is capable of enhancing the energy harvesting performance of the single pendulum harvester. Similar to the calculated results of the spring pendulum system, the calculated results of the single pendulum possess a larger peak value when the internal friction is not considered.

4.2. Maximum output

To evaluate the maximum output power of the proposed dual EMEHs, both the spring pendulum system and single pendulum system are measured with the resonance frequency (0.85 Hz) and increasing excitation amplitudes.

4.2.1. Spring pendulum system

With the increasing excitation amplitudes, the output power of the spring pendulum system is extracted through the measured voltage as shown in Fig. 10. With the excitation amplitude of $A = 150$ mm (acceleration is equal to 0.29 g), the output power is around 450 mW for both H_1 and H_2. The total output power is around 900 mW, which reaches the level of Watt. Since the transduction factor is increasing with its dimension [3], large replaceable EMEHs would yield even higher harvesting performance. The output power of H_1 is monotonically

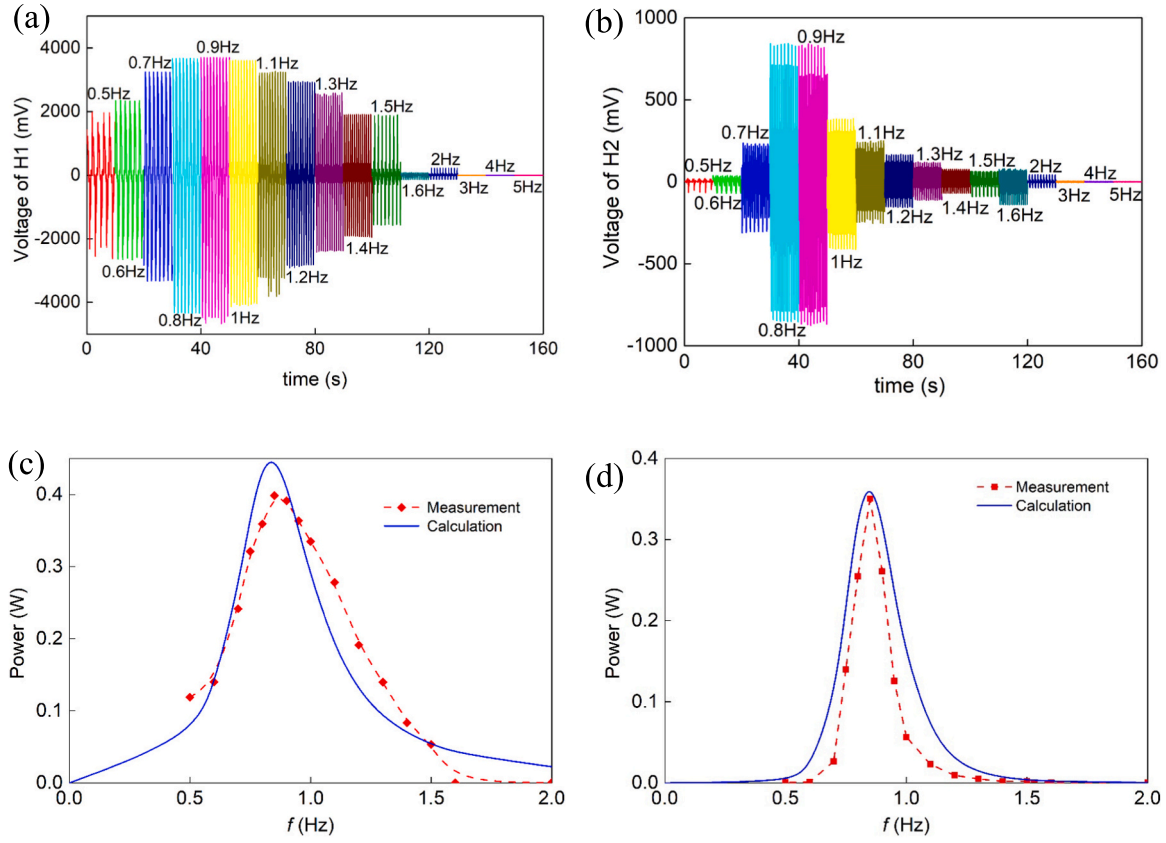

Fig. 8. Dual-EMEHs output in the spring pendulum system: (a) Output voltage of H_1; (b) output voltage of H_2; (c) output power of H_1 with varied excitation frequencies, (d) output power of H_2 with varied excitation frequencies.

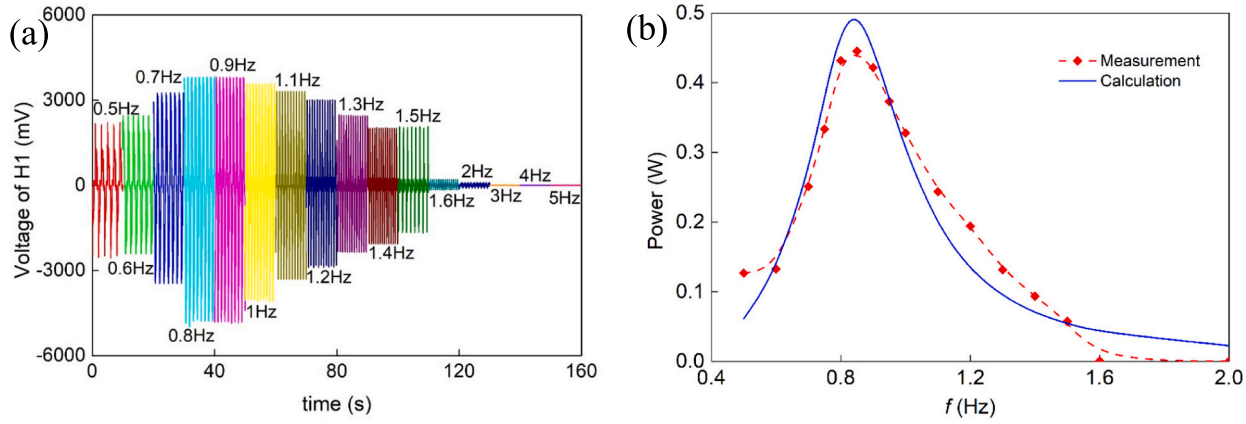

Fig. 9. H_1 in single pendulum system: (a) Output voltage; (b) output power with varied excitation frequency.

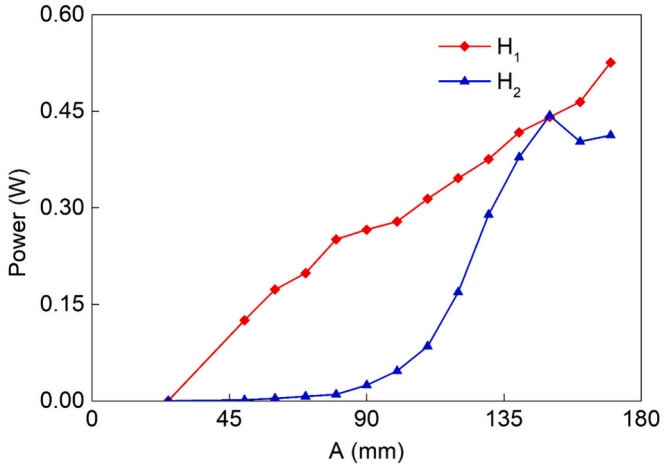

Fig. 10. Output power of dual-EMEHs with different excitation amplitudes in spring pendulum system under 0.85 Hz excitation.

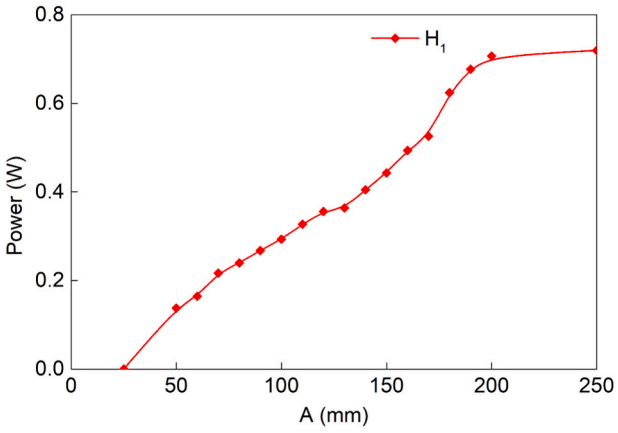

Fig. 11. Output power of H_1 with different excitation amplitudes in the single pendulum system under 0.85 Hz excitation.

increasing with the excitation amplitude A. However, the output power of H_2 possesses a peak point at $A \approx 150$ mm. The decreasing reason after the peak point is that the vibration amplitude exceeds its effective working range. Reaching $A \approx 175$ mm, the vibration amplitude is too large so that impact occurs between the eyebolt and the limiting plates in Fig. 3(d). When $A > 150$ mm, the output voltage of H_2 is not a regular sinusoidal wave that can hardly be utilized by electrical appliances directly. Compared with a single pendulum system, the spring pendulum system with the added translational DOF contains lower stiffness, which contributes to the large working stroke of the added DOF. Therefore, the maximum excitation amplitude is limited to avoid impact damage to internal structures.

Moreover, this impact phenomenon can also trigger the overloading situation with large ocean wave excitation. To avoid possible destruction of the proposed harvester in this kind of harsh situation, the damping coefficient can be increased by decreasing tunable resistance R_1 and R_2. The tuning strategy will decrease the output power but safeguard the equipment. After the harsh excitation is over, the external resistance can be tuned back to the optimal matching resistance.

4.2.2. Single pendulum system

Similar to the constant acceleration excitation test, a comparative experiment of the single pendulum is conducted to reach its maximum output power with the increasing excitation amplitude. As shown in Fig. 11, the output power with $A = 150$ mm is 450 mW, which is near the H_1 output in the spring pendulum system but only half of the total output power. If the excitation amplitude increases to $A = 250$ mm, the output power will be increased to around 720 mW, which is larger than the H_1 output in the spring pendulum system but still less than the total output power with even smaller excitation. Moreover, when the single pendulum is excited with larger amplitudes, the increase in the output power slows down. The reason is that the pendulum period increases with the swing angle due to the nonlinear variation relationship between them. Therefore, when the swing angle is sufficiently large (90°,180°), the pendulum response is not suitable for energy harvesting. The pendulum-like system strives to cross the unstable equilibrium point at 180°, then the swing motion is converted into a circular motion. This might inspire a different design in future research.

To the best of the authors' knowledge, the output power with the proposed dual EMEHs is larger than the ones from similar pendulum-like harvesters of the same magnitude reported in the literature. For better comparison, the power density that informs on the output power per unit volume is calculated. The total volume of the two converters is 117.07 cm^3, namely 20.61 cm^3 for H_1 and 96.46 cm^3 for H_2, based on the dimensions tabulated in Table 1. To achieve a fair comparison, in the single pendulum system, H_2 acts as a proof mass whose volume is also included in the estimation of the total volume. The calculated output power densities are 7.68 mW/cm^3 and 6.15 mW/cm^3 for the spring pendulum system and the single pendulum system, respectively. Therefore, compared with the single pendulum, the spring pendulum offers higher energy output, a wider frequency output bandwidth, and effective energy output with the vertical motion excitation arising from the ocean wave heave motion.

5. Conclusions

Dual EMEHs design in spring pendulum structure is proposed in this paper for ultra-low frequency vibration energy harvesting. A rotational EMEH is in charge of harvesting the swinging energy and a translational EMEH of the linear vibration energy. To identify the system variables and compare the performance, the degenerative single pendulum system with one DOF is used by locking the relative motion of the translational EMEH. Theoretical and numerical analyses are performed on both systems through system modeling based on Lagrange's equation.

Experiments on both systems are conducted to verify and compare their respective energy harvesting performances. The structural parameters are identified step by step with several pre-tests. Then, the excitations with constant acceleration (swept sinusoidal waves) and constant frequency (increasing amplitudes) are implemented on both systems to elucidate the harvested energy. Experimental results with constant acceleration excitation confirm the effectiveness of the spring pendulum structural design. Dual EMEHs in the spring pendulum system can harvest higher energy (0.75 W) than that in the single pendulum system (0.45 W) with a 0.2 g excitation. Moreover, the spring mass oscillator, vibrating due to internal resonance, can trigger the frequency up-conversion feature while suppressing the swing angle of the main system. The measured maximum output power is doubled when the single pendulum system is changed as the spring pendulum system under the excitation (0.85 Hz, 0.29 g). The tunable damping of the dual EMEHs can protect the equipment from destruction under harsh situations.

CRediT authorship contribution statement

Ruqi Sun: Writing – original draft, Validation, Software, Methodology, Investigation, Funding acquisition, Data curation, Conceptualization. **Shengxi Zhou:** Writing – review & editing, Supervision, Resources, Project administration, Funding acquisition, Formal analysis. **Zhongjie Li:** Writing – review & editing, Validation, Supervision, Methodology, Investigation, Funding acquisition, Formal analysis. **Li Cheng:** Writing – review & editing, Supervision, Methodology, Investigation, Formal analysis.

Declaration of competing interest

The authors declare that they have no known competing financial interests or personal relationships that could have appeared to influence the work reported in this paper.

Data availability

Data will be made available on request.

Acknowledgments

This work was supported by the Fundamental Research Funds for the Central Universities, CHD (Grant No. 300102223108), the National Natural Science Foundation of China (Grant No. 12072267), the Fundamental Research Funds for the Central Universities (Grant No. D5000230099), Shanghai Science and Technology Committee (Grant No. 22dz1204300). The authors would like to thank Mr. Zhiyuan Li for conversation about the mathematic modeling.

Appendix A. Motion equation of the damped spring pendulum

For the damped spring pendulum Lagrange equation derivation, with the coordinate decomposition and variables substitution, the total kinetic energy of m_1 and m_2 becomes:

$$T=\frac{1}{2}m_1\left(l_1^2\dot{\theta}^2+\dot{s}^2-2l_1cos\theta\bullet\dot{\theta}\bullet\dot{s}\right)+\frac{1}{2}m_2\left\{(l_2+r)^2\dot{\theta}^2+\dot{r}^2+\dot{s}^2-2\dot{s}\left[(l_2+r)cos\theta\bullet\dot{\theta}+\dot{r}\bullet sin\theta\right]\right\} \tag{A1}$$

The gravitational and elastic potential energy can be written as:

$$U=-m_1gl_1cos\theta-m_2g(l_2+r)cos\theta+\frac{1}{2}k\left(r+\frac{m_2g}{k_2}\right)^2 \tag{A2}$$

For the coordinate θ, corresponding components in Eq. (1) can be deduced, as follows:

$$\frac{\partial T}{\partial\dot{\theta}}=m_1l_1^2\dot{\theta}-m_1l_1\dot{s}cos\theta+m_2(l_2+r)^2\dot{\theta}-m_2(l_2+r)\dot{s}cos\theta \tag{A3}$$

$$\frac{d}{dt}\left(\frac{\partial T}{\partial\dot{\theta}}\right)=\left[m_1l_1^2+m_2(l_2+r)^2\right]\ddot{\theta}-[m_1l_1+m_2(l_2+r)]cos\theta\ddot{s}+[m_1l_1+m_2(l_2+r)]\dot{s}\dot{\theta}sin\theta+2m_2(l_2+r)\dot{r}\dot{\theta}-m_2\dot{r}\dot{s}cos\theta \tag{A4}$$

$$\frac{\partial T}{\partial\theta}=[m_1l_1+m_2(l_2+r)]\dot{s}\dot{\theta}sin\theta-m_2\dot{r}\dot{s}cos\theta \tag{A5}$$

$$\frac{\partial U}{\partial\theta}=m_1gl_1sin\theta+m_2g(l_2+r)sin\theta \tag{A6}$$

$$\frac{\partial D}{\partial\dot{\theta}}=c_1\dot{\theta} \tag{A7}$$

For the coordinate r, corresponding components in Eq. (1) can be deduced, as follows:

$$\frac{\partial T}{\partial\dot{r}}=m_2\dot{r}-m_2\dot{s}sin\theta \tag{A8}$$

$$\frac{d}{dt}\left(\frac{\partial T}{\partial\dot{r}}\right)=m_2\ddot{r}-m_2\ddot{s}sin\theta-m_2\dot{s}\dot{\theta}cos\theta \tag{A9}$$

$$\frac{\partial T}{\partial r} = m_2(l_2 + r)\dot{\theta}^2 - m_2\dot{s}\dot{\theta}cos\theta \tag{A10}$$

$$\frac{\partial U}{\partial r} = kr + m_2 g - m_2 gcos\theta \tag{A11}$$

$$\frac{\partial D}{\partial \dot{r}} = c_2\dot{r} \tag{A12}$$

Then, taking Eqs. (A3) ~ (A12) into Eq. (1), the Lagrange equation of m_1 and m_2 can be obtained as Eqs. (5) and (6).

Appendix B. Motion equation of the single spring pendulum

For the damped spring pendulum Lagrange equation derivation, the kinetic energy of total mass m can be expressed as:

$$T = \frac{1}{2}m\left(l^2\dot{\theta}^2 + \dot{s}^2 - 2lcos\theta \bullet \dot{\theta} \bullet \dot{s}\right) \tag{B1}$$

Concerning the only variable θ, corresponding components in Eq. (1) can be deduced as:

$$\frac{\partial T}{\partial \dot{\theta}} = ml^2\dot{\theta} - mlcos\theta \bullet \dot{s} \tag{B2}$$

$$\frac{d}{dt}\left(\frac{\partial T}{\partial \dot{\theta}}\right) = ml^2\ddot{\theta} + mlsin\theta \bullet \dot{\theta} \bullet \dot{s} - mlcos\theta \bullet \ddot{s} \tag{B3}$$

$$\frac{\partial T}{\partial \theta} = mlsin\theta \bullet \dot{\theta} \bullet \dot{s} \tag{B4}$$

$$\frac{\partial U}{\partial \theta} = mglsin\theta \tag{B5}$$

$$\frac{\partial D}{\partial \dot{\theta}} = c_1\dot{\theta} \tag{B6}$$

Then, taking Eqs.(B1) ~ (B6) into Eq. (1), the Lagrange equation of m can be obtained as Eq. (12).

References

[1] Scruggs J, Jacob P. Harvesting ocean wave energy. Science 2009 Feb 27;323 (5918):1176–8.
[2] Aderinto T, Li H. Ocean wave energy converters: status and challenges. Energies 2018 May 14;11(5):1250.
[3] Sun R, Zhou S, Cheng L. Ultra-low frequency vibration energy harvesting: mechanisms, enhancement techniques, and scaling laws. Energ Conver Manage 2023 Jan 15;276:116585.
[4] Li H, Tian C, Deng ZD. Energy harvesting from low frequency applications using piezoelectric materials. Appl Phys Rev 2014 Dec 1;1(4).
[5] Muscat A, Bhattacharya S, Zhu Y. Electromagnetic vibrational energy harvesters: a review. Sensors 2022 Jul 25;22(15):5555.
[6] Rodrigues C, Nunes D, Clemente D, Mathias N, Correia JM, Rosa-Santos P, et al. Emerging triboelectric nanogenerators for ocean wave energy harvesting: state of the art and future perspectives. Energ Environ Sci 2020;13(9):2657–83.
[7] Zhao LC, Zou HX, Zhao YJ, Wu ZY, Liu FR, Wei KX, et al. Hybrid energy harvesting for self-powered rotor condition monitoring using maximal utilization strategy in structural space and operation process. Appl Energy 2022 May 15;314:118983.
[8] Zhang B, Liu H, Zhou S, Gao J. A review of nonlinear piezoelectric energy harvesting interface circuits in discrete components. Appl Math Mech 2022 Jul;43 (7):1001–26.
[9] Yan G, Wu ZY, Wei XS, Wang S, Zou HX, Zhao LC, et al. Nonlinear compensation method for quasi-zero stiffness vibration isolation. J Sound Vib 2022 Apr 14;523: 116743.
[10] Ling P, Miao L, Ye B, You J, Zhang W, Yan B. Ultra-low frequency vibration isolation of a novel click-beetle-inspired structure with large quasi-zero stiffness region. J Sound Vib 2023 Aug 18;558:117756.
[11] Ye K, Ji JC, Brown T. Design of a quasi-zero stiffness isolation system for supporting different loads. J Sound Vib 2020 Apr 14;471:115198.
[12] Hao RB, Lu ZQ, Ding H, Chen LQ. Orthogonal six-DOFs vibration isolation with tunable high-static-low-dynamic stiffness: experiment and analysis. Int J Mech Sci 2022 May 15;222:107237.
[13] Li M, Jing X. Novel tunable broadband piezoelectric harvesters for ultralow-frequency bridge vibration energy harvesting. Appl Energy 2019 Dec 1;255: 113829.
[14] Wang K, Zhou J, Ouyang H, Chang Y, Xu D. A dual quasi-zero-stiffness sliding-mode triboelectric nanogenerator for harvesting ultralow-low frequency vibration energy. Mech Syst Signal Process 2021 Apr 1;151:107368.
[15] Luo H, Liu J, Yang T, Zhang Y, Cao Q. Dipteran flight-inspired bistable triboelectric nanogenerator for harvesting low frequency vibration. Nano Energy 2022 Dec 1; 103:107755.
[16] Fang S, Chen K, Lai Z, Zhou S, Yurchenko D, Liao WH. A bio-inspired system for simultaneous vibration isolation and energy harvesting in post-capture spacecraft. Mech Syst Signal Process 2023 Sep 15;199:110466.
[17] Fang S, Chen K, Zhao B, Lai Z, Zhou S, Liao WH. Simultaneous broadband vibration isolation and energy harvesting at low frequencies with quasi-zero stiffness and nonlinear monostability. J Sound Vib 2023 Jun 9;553:117684.
[18] Chen Z, Chen Z, Wei Y. Quasi-zero stiffness-based synchronous vibration isolation and energy harvesting: a comprehensive review. Energies 2022 Sep 26;15(19): 7066.
[19] Fan K, Tan Q, Liu H, Zhang Y, Cai M. Improved energy harvesting from low-frequency small vibrations through a monostable piezoelectric energy harvester. Mech Syst Signal Process 2019 Feb 15;117:594–608.
[20] Erturk A, Inman DJ. Broadband piezoelectric power generation on high-energy orbits of the bistable Duffing oscillator with electromechanical coupling. J Sound Vib 2011 May 9;330(10):2339–53.
[21] Zhou J, Zhao X, Wang K, Chang Y, Xu D, Wen G. Bio-inspired bistable piezoelectric vibration energy harvester: design and experimental investigation. Energy 2021 Aug 1;228:120595.
[22] Tan D, Zhou J, Wang K, Zhao X, Wang Q, Xu D. Bow-type bistable triboelectric nanogenerator for harvesting energy from low-frequency vibration. Nano Energy 2022 Feb 1;92:106746.
[23] Tan D, Zhou J, Wang K, Ouyang H, Zhao H, Xu D. Sliding-impact bistable triboelectric nanogenerator for enhancing energy harvesting from low-frequency intrawell oscillation. Mech Syst Signal Process 2023 Feb 1;184:109731.
[24] Liu Q, Cao J, Zhang Y, Zhao Z, Kerschen G, Jing X. Interpretable sparse identification of a bistable nonlinear energy sink. Mech Syst Signal Process 2023 Jun 15;193:110254.
[25] Zhou S, Cao J, Inman DJ, Lin J, Liu S, Wang Z. Broadband tristable energy harvester: modeling and experiment verification. Appl Energy 2014 Nov 15;133: 33–9.
[26] Litak G, Wolszczak P, Caban J, Margielewicz J, Gąska D, Ma X, et al. Energy harvesting using a nonlinear resonator with asymmetric potential Wells. Energies 2022 Dec 14;15(24):9469.
[27] Zhou S, Zuo L. Nonlinear dynamic analysis of asymmetric tristable energy harvesters for enhanced energy harvesting. Commun Nonlinear Sci Numer Simul 2018 Aug 1;61:271–84.
[28] Zhou S, Lallart M, Erturk A. Multistable vibration energy harvesters: principle, progress, and perspectives. J Sound Vib 2022 Jun 23;528:116886.
[29] Fang S, Zhou S, Yurchenko D, Yang T, Liao WH. Multistability phenomenon in signal processing, energy harvesting, composite structures, and metamaterials: a review. Mech Syst Signal Process 2022 Mar 1;166:108419.

[30] Deng H, Du Y, Wang Z, Ye J, Zhang J, Ma M, et al. Poly-stable energy harvesting based on synergetic multistable vibration. Commun Phys 2019 Feb 26;2(1):21.
[31] Zhang Y, Liao WH, Bowen C, Wang W, Cao J. Applicability of magnetic force models for multi-stable energy harvesters. J Intell Mater Syst Struct 2023 May;34 (9):1104–20.
[32] Wang W, Li B, Liu S, Wei ZH. Bifurcation analysis and nonlinear dynamics of a rolling magnet multistable electromagnetic energy harvester. Commun Nonlinear Sci Numer Simul 2023 Apr 1;118:107027.
[33] Fu H, Jiang J, Hu S, Rao J, Theodossiades S. A multi-stable ultra-low frequency energy harvester using a nonlinear pendulum and piezoelectric transduction for self-powered sensing. Mech Syst Signal Process 2023 Apr 15;189:110034.
[34] Song R, Hou C, Yang C, Yang X, Guo Q, Shan X. Modeling, validation, and performance of two tandem cylinder piezoelectric energy harvesters in water flow. Micromachines 2021 Jul 25;12(8):872.
[35] Zhao LC, Zou HX, Xie X, Guo DH, Gao QH, Wu ZY, et al. Mechanical intelligent wave energy harvesting and self-powered marine environment monitoring. Nano Energy 2023 Apr 1;108:108222.
[36] Shen W, Sun Z, Hu Y, Cai L, Zhu H, Silva S. Energy harvesting performance of an inerter-based electromagnetic damper with application to stay cables. Mech Syst Signal Process 2022 May 1;170:108790.
[37] Tan Q, Fan K, Tao K, Zhao L, Cai M. A two-degree-of-freedom string-driven rotor for efficient energy harvesting from ultra-low frequency excitations. Energy 2020 Apr 1;196:117107.
[38] Ma X, Fan K, Zhang X, Zhao S, He H, Zhang C, et al. A snap-through vibration-rotation modulation mechanism for high-performance low frequency energy harvester. Mech Syst Signal Process 2023 Nov 1;202:110717.
[39] Marszal M, Witkowski B, Jankowski K, Perlikowski P, Kapitaniak T. Energy harvesting from pendulum oscillations. Int J Non-Linear Mech 2017 Sep 1;94: 251–6.
[40] Lu Z, Zhao L, Ding H, Chen LQ. A dual-functional metamaterial for integrated vibration isolation and energy harvesting. J Sound Vib 2021 Sep 29;509:116251.
[41] Kumar R, Gupta S, Ali SF. Energy harvesting from chaos in base excited double pendulum. Mech Syst Signal Process 2019 Jun 1;124:49–64.
[42] Wang T. Pendulum-based vibration energy harvesting: mechanisms, transducer integration, and applications. Energ Conver Manage 2023 Jan 15;276:116469.
[43] Chen LQ, Jiang WA. Internal resonance energy harvesting. J Appl Mech 2015 Mar 1;82(3):031004.
[44] Jiang WA, Chen LQ, Ding H. Internal resonance in axially loaded beam energy harvesters with an oscillator to enhance the bandwidth. Nonlinear Dyn 2016 Sep; 85:2507–20.
[45] Xu J, Tang J. Multi-directional energy harvesting by piezoelectric cantilever-pendulum with internal resonance. Appl Phys Lett 2015;107(21).
[46] Xiong L, Tang L, Mace BR. Internal resonance with commensurability induced by an auxiliary oscillator for broadband energy harvesting. Appl Phys Lett 2016 May 16;108(20).
[47] Nie X, Pei S, Tan T, Yan Z, Yan Z. Nonlinear 1: 2 internal resonance response of L-shaped piezoelectric energy harvester under the influence of electrical damping. Int J Mech Sci 2022 Jul 1;225:107365.
[48] Kane TR, Kahn ME. On a class of two-degree-of-freedom oscillations. J Appl Mech 1968 Sep;35(3):547–52.
[49] Narkis Y. On the stability of a spring-pendulum. Zeitschrift für angewandte Mathematik und Physik ZAMP 1977 Mar;28(2):343–8.
[50] Miles JW. On internal resonance of two damped oscillators. Stud Appl Math 1976 Dec;55(4):351–9.
[51] Broucke R, Baxa PA. Periodic solutions of a spring-pendulum system. Celest Mech 1973 Sep;8(2):261–7.
[52] Gitterman M. Spring pendulum: parametric excitation vs an external force. Physica A 2010 Aug 15;389(16):3101–8.
[53] Baleanu D, Jajarmi A, Asad J. The fractional model of spring pendulum: newfeatures within different kernels, proceedings of the Romanian academy. Series A 2018;19:447–54.
[54] Abohamer MK, Awrejcewicz J, Starosta R, Amer TS, Bek MA. Influence of the motion of a spring pendulum on energy-harvesting devices. Appl Sci 2021 Sep 17; 11(18):8658.
[55] De Sousa MC, Marcus FA, Caldas IL, Viana RL. Energy distribution in spring pendulum. Nonlinear Optics 2017;4(6).
[56] Amer TS, Bek MA. Chaotic responses of a harmonically excited spring pendulum moving in circular path. Nonlinear Anal Real World Appl 2009 Oct 1;10(5): 3196–202.
[57] Amer TS, Bek MA, Abouhmr MK. On the vibrational analysis for the motion of a harmonically damped rigid body pendulum. Nonlinear Dyn 2018 Mar;91: 2485–502.
[58] Kecik K, Borowiec M. An autoparametric energy harvester. Eur Phys J Spec Top 2013 Sep;222(7):1597–605.
[59] Mitura A, Kecik K. Influences of system parameters on energy harvesting from autoparametric absorber. Experimental Res Vibr Phys Syst 2016;27:287–91.
[60] Kecik K, Mitura A. Theoretical and experimental investigations of a pseudo-magnetic levitation system for energy harvesting. Sensors 2020 Mar 14;20(6): 1623.
[61] Jiang W, Han X, Chen L, Bi Q. Improving energy harvesting by internal resonance in a spring-pendulum system. Acta Mech Sin 2020 Jun;36:618–23.
[62] Wu Y, Qiu J, Zhou S, Ji H, Chen Y, Li S. A piezoelectric spring pendulum oscillator used for multi-directional and ultra-low frequency vibration energy harvesting. Appl Energy 2018 Dec 1;231:600–14.
[63] Wu Y, Li S, Fan K, Ji H, Qiu J. Investigation of an ultra-low frequency piezoelectric energy harvester with high frequency up-conversion factor caused by internal resonance mechanism. Mech Syst Signal Process 2022 Jan 1;162:108038.
[64] He CH, Amer TS, Tian D, Abolila AF, Galal AA. Controlling the kinematics of a spring-pendulum system using an energy harvesting device. J Low Frequency Noise Vibr Active Control 2022 Sep;41(3):1234–57.
[65] Kecik K. Assessment of energy harvesting and vibration mitigation of a pendulum dynamic absorber. Mech Syst Signal Process 2018 Jun 1;106:198–209.
[66] Kecik K, Mitura A. Energy recovery from a pendulum tuned mass damper with two independent harvesting sources. Int J Mech Sci 2020 May 15;174:105568.
[67] Kecik K. Numerical study of a pendulum absorber/harvester system with a semi-active suspension. ZAMM-Journal of Applied Mathematics and Mechanics/ Zeitschrift für Angewandte Mathematik und Mechanik 2021 Jan;101(1): e202000045.
[68] Sun R, Wong W, Cheng L. Optimal design of a tunable electromagnetic shunt damper for dynamic vibration absorber. Mechatronics 2022 May 1;83:102763.
[69] Sun R, Wong W, Cheng L. Bi-objective optimal design of an electromagnetic shunt damper for energy harvesting and vibration control. Mech Syst Signal Process 2023 Jan 1;182:109571.